Biochemical Journal (2018) **475** 3949–3962
https://doi.org/10.1042/BCJ20180769

Research Article

Structure of the sensory domain of McpX from *Sinorhizobium meliloti*, the first known bacterial chemotactic sensor for quaternary ammonium compounds

Manisha Shrestha[1], Karl K. Compton[1], Jordan M. Mancl[1], Benjamin A. Webb[1], Anne M. Brown[2], Birgit E. Scharf[1] and Florian D. Schubot[1]

[1]Department of Biological Sciences, Virginia Tech, Derring Hall, Blacksburg, VA 24061, U.S.A.; [2]Department of Biochemistry, Virginia Tech, Engel Hall, Blacksburg, VA 24061, U.S.A.

Correspondence: Birgit E. Scharf (bscharf@vt.edu) or Florian D. Schubot (fschubot@vt.edu)

The α-proteobacterium *Sinorhizobium meliloti* can live freely in the soil or engage in a symbiosis with its legume host. *S. meliloti* facilitates nitrogen fixation in root nodules, thus providing pivotal, utilizable nitrogen to the host. The organism has eight chemoreceptors, namely McpT to McpZ and IcpA that facilitate chemotaxis. McpX is the first known bacterial sensor of quaternary ammonium compounds (QACs) such as choline and betaines. Because QACs are exuded at chemotaxis-relevant concentrations by germinating alfalfa seeds, McpX has been proposed to contribute to host-specific chemotaxis. We have determined the crystal structure of the McpX periplasmic region ($McpX^{PR}$) in complex with the proline betaine at 2.7 Å resolution. In the crystal, the protein forms a symmetric dimer with one proline betaine molecule bound to each monomer of $McpX^{PR}$ within membrane-distal CACHE module. The ligand is bound through cation–πinteractions with four aromatic amino acid residues. Mutational analysis in conjunction with binding studies revealed that a conserved aspartate residue is pivotal for ligand binding. We discovered that, in a striking example of convergent evolution, the ligand-binding site of $McpX^{PR}$ resembles that of a group of structurally unrelated betaine-binding proteins including ProX and OpuAC. Through this comparison and docking studies, we rationalized the specificity of $McpX^{PR}$ for this specific group of ligands. Collectively, our structural, biochemical, and molecular docking data have revealed the molecular determinants in McpX that are crucial for its rare ligand specificity for QACs.

Introduction

Bacteria utilize a wide range of naturally occurring organic compounds as sources for carbon, nitrogen, and for the fundamental building blocks required for the synthesis of proteins, lipids, and nucleic acids. To identify and seek out diverse nutrient sources and eukaryotic hosts, many bacteria have evolved a mechanism to link their swimming motility with a complex chemosensory system [1–3]. This process, called chemotaxis, entails the coupling of the chemotactic sensory machinery with the rotation of the flagella and thus swimming motility. Chemotactic behavior is best understood in *Escherichia coli*, which uses several perichtrichous flagella to form a bundle for propulsion [4]. The canonical sensing mechanism for environmental signals involves signal recognition by chemoreceptors called methyl-accepting chemotaxis proteins (MCPs), which typically consist of two transmembrane domains, a variable periplasmic ligand-binding domain, and a conserved cytoplasmic signaling domain [5]. MCPs form a ternary complex with the adaptor protein CheW

Received: 21 September 2018
Revised: 7 November 2018
Accepted: 14 November 2018

Accepted Manuscript online: 15 November 2018
Version of Record published: 14 December 2018

Biochemical Journal (2018) **475** 3949–3962
https://doi.org/10.1042/BCJ20180769

that mediates binding the MCPs to the histidine autokinase CheA [6]. In the absence of a chemoattractant or in the presence of a repellent, CheA autophosphorylates and then transfers the phosphate group to its cognate response regulator CheY. Phosphorylated CheY binds to the flagellar motor to cause a disruption of the flagellar bundle resulting in bacterial cell tumble and thus random reorientation [7,8]. Binding of a chemoattractant to its cognate MCP induces a conformational change in the sensory domain to produce a piston-type motion accompanied by a twisting motion across the cellular membrane, which alters the conformation of the kinase control region. This structural change reduces the activity of CheA, thus slowing the rate of CheY phosphorylation and thereby reducing the tumble frequency of the cell. The overall outcome is a biased random walk of the bacterial cell toward the source of the detected attractant or away from a repellent [5].

MCPs are obligate dimers, which form trimers of dimers and further organize into large-scale arrays at the cell pole that are composed of MCPs with differing ligand specificities [9]. These arrays serve to amplify the signal originating from individual ligand-bound MCPs to increase the sensitivity of the system [10]. The associated conformational change cascades across the array to induce similar structural changes in receptors without a bound ligand [11]. The chemotactic response is further modulated through the reversible methylation of conserved sites in the cytosolic region of MCPs. A constitutively active methyltransferase adds methyl groups, while a methylesterase removes methyl groups after it is activated through phosphorylation by CheA. Methylation creates a memory of recent ligand-binding events and provides an adaptive mechanism to prevent saturation of the chemotaxis system as the bacterium swims up a nutrient gradient. Attractant binding reduces CheA activity but also stimulates the gradual methylation of the MCP, which in turn increases CheA activity leading to a gradual recovery of the tumble frequency [12]. This adaptive mechanism thereby reduces the sensitivity of the MCP array and ensures that only a further increased chemoattractant concentration will produce a chemotactic response to guide the bacterial cell further up the gradient.

Chemotaxis enables the soil-dwelling plant symbiont *Sinorhizobium meliloti* to actively seek the suitable site for host root infection [13–15]. It possesses eight distinct chemoreceptors sequentially named McpT to McpZ and IcpA, which lacks the conserved methylation sites, to sense environmental cues [16]. IcpA and McpY do not have transmembrane regions but still associate with the chemoreceptor cluster at the cell poles [17]. It is hypothesized that these two chemoreceptors sense compounds that have been internalized or could be used as energy level sensors by somehow sensing the energy flux in the cell [15]. Signal sensing for the six transmembrane MCPs is based on chemoreception in the periplasm. The ligand-binding specificity of two of the eight *S. meliloti* chemoreceptors involved in chemotaxis has been determined. McpU is a general amino acid receptor, sensing all non-acidic proteogenic amino acids, as well as several non-proteogenic amino acids [18–20]. McpX senses quaternary ammonium compounds (QACs) such as glycine betaine, proline betaine, trigonelline, and choline [21]. *S. meliloti* utilizes proline betaine as a nutrient source but various microorganisms accumulate these compounds inside the cell to counter stress caused by high osmolarity and extremes in growth temperature [22]. Amino acids and QACs are commonly exuded by plant seeds and roots including those of alfalfa, the plant symbiont of *S. meliloti* [19,21]. The periplasmic regions of MCPs may be classified according to the predicted folds of their domains, and in some instances, a particular domain fold may be predictive of the MCPs specificity. The periplasmic regions of McpU and McpX were predicted to each contain a dual CACHE domain (dCACHE_1), an arrangement frequently encountered in amino acid sensors [23]. Mutational analyses and molecular modeling have shown that amino acid ligands bind to the amino-proximal CACHE module in McpU [20]. Profiling of the ligand specificity of McpX revealed that, in addition to QACs, it only binds one amino acid with significant affinity, namely proline [21,24–26]. Therefore, the ligand specificity of McpX may play a role in promoting symbiosis.

In the present study, we report the crystal structure of the McpX ligand-binding periplasmic region ($McpX^{PR}$) in complex with the betaine proline betaine. The structure revealed striking similarities between the ligand-binding pocket of McpX and that found in a structurally unrelated group of QAC-binding proteins. Our structural analysis was used to explain how McpX reconciles having a strong selectivity for QACs with maintaining a broad affinity for compounds as chemically distinct as choline and proline betaine. Collectively, this work uncovered a remarkable example of convergent evolution and offers intriguing insights into nature's design principles for achieving specificity through subtle modifications in binding pocket properties. Ultimately, understanding these principles may enable us rationally engineer novel specificities to gain control of bacterial chemotaxis.

Biochemical Journal (2018) **475** 3949–3962
https://doi.org/10.1042/BCJ20180769

Materials and methods

Chemicals

Proline betaine (L-proline betaine) was purchased from Extrasynthese (Toulouse, France) and choline from Sigma-Fluka (St. Louis, MO, U.S.A.).

Expression and purification of the periplasmic region of McpX ($McpX^{PR}$) and crystallization

The *mcpX* 100–919 bp fragment was amplified with Phusion DNA polymerase (NEBiolabs) using chromosomal DNA as template and cloned into Qiagen expression vector pQE30 using *Bam*HI and *Hin*dIII sites to produce the expression plasmid pBS455, wherein an N-terminal His_6-tag is fused in frame with the codons for amino acid residues 34–306 of the *mcpX* gene. The clone was verified using DNA sequencing with pQE30-specific primers. The recombinant ligand-binding, a periplasmic region of McpX ($McpX^{PR}$, $McpX_{34–306}$) was overproduced from plasmid pBS455 in *E. coli* M15/pREP4 cell. Four liters of cell culture was grown to an OD_{600} of 0.7 at 37°C in LB containing 100 μg ml^{-1} ampicillin and 25 μg ml^{-1} kanamycin. Gene expression was induced by the addition of 0.6 mM isopropyl-β-D-thiogalactopyranoside for 4 h at 25°C. Cells were harvested via centrifugation and stored at −30°C. Cells were suspended in 70 ml column buffer [500 mM NaCl, 25 mM imidazole, 20 mM $NaPO_4$, pH 7.4, 2 mM tri(2-carboxyethyl)phosphine (TCEP), 1 mM phenylmethylsulfonyl fluoride (PMSF)] with 1 μg/ml of DNase and lysed by three passages through a French pressure cell at 20 000 psi (SLM Aminco, Silver Spring, MD, U.S.A.). The soluble fraction was loaded onto three stacked 5 ml NTA columns (GE Healthcare Life Sciences) charged with Ni^{2+}. Protein was eluted from the column in a linear gradient of elution buffer (500 mM NaCl, 350 mM imidazole, 20 mM $NaPO_4$, pH 7.0, 2 mM TCEP, 1 mM PMSF). Protein-containing fractions were pooled and loaded onto a HiPrep 26/60 Sephacryl S-300 HR (GE Healthcare) gel filtration column. Prior, this column had been equilibrated in column buffer containing 100 mM NaCl, 50 mM HEPES, pH 7.0. Peak fractions were analyzed via SDS–PAGE. Fractions containing >95% purified $McpX^{PR}$ were pooled and concentrated via ultrafiltration with 10-kDa cutoff regenerated cellulose membranes in a 50 ml Amicon filter unit (Millipore, Bedford, MA, U.S.A.), and stored at 4°C.

The change of Asp208 to Asn was introduced into *mcpX* using overlap extension PCR followed by the same cloning steps that had been used for the generation of pBS455 except that the parental plasmid was pQE60, creating pBS517. Subsequent expression and purification steps of the Asp208Asn $McpX^{PR}$ variant ($McpX^{D208N\text{-}PR}$) mirrored those used for the purification of the original $McpX^{PR}$ protein. $McpX^{D208N\text{-}PR}$ behaved identically to the original protein during sample purification and concentration. In a preliminary differential scanning fluorimetry experiment, the protein did not show binding to proline betaine but produced a sharp melting transition curve characteristic of a folded and homogeneous sample (not shown).

Initial crystals of $McpX^{PR}$ in the presence of proline betaine were obtained through high-throughput screening of commercial crystallization conditions using a sitting drop format and a Honeybee961 crystallization robot. Optimized crystals were obtained in a hanging drop set-up by combining 3 μl protein solutions containing 190 μM $McpX^{PR}$, 9 mM proline betaine, 100 mM NaCl, and 50 mM HEPES, pH 7.0 with 1 μl of a screening condition containing 0.08 M sodium acetate, 1.6 M ammonium sulfate, and 20% glycerol, pH 4.6. The droplet was allowed to equilibrate at room temperature against a reservoir containing 64 mM sodium acetate, 1.28 M ammonium sulfate, and 16% glycerol, pH 4.6. Crystals appeared within a day. Many crystals displaying a wheel-like shape proved to be twinned but others, displaying a topology more reflective of their tetrahedral lattice system, yielded untwinned diffraction data to ∼2.7 Å.

X-ray diffraction data collection, structure determination, and refinement

X-ray data at 2.7 Å were collected at SER-CAT 22-ID at the Advanced Photon Source in Argonne, Il using a MARMOSAIC 300 CCD detector. The X-ray diffraction data were processed using the HKL2000 program package. Data were analyzed with Xtriage from the PHENIX program suite [27] to confirm that the crystals were not twinned. Initial phases were obtained with molecular replacement using the structure of the extracellular domain of the putative histidine kinase mmHK1S-Z3 as a search model (PDB code: 3lib). PHASER from within the PHENIX program suite was used for the search and to calculate the initial density map. Model building was performed using COOT, and the PHENIX program suite was used for model refinement [27]. During the refinement, the diffraction data were cut off at 2.7 Å using the correlation of the observed data set with the refined model, CC1/2, as defined by Karplus and Diederichs as selection criterion [28]. Data collection

Biochemical Journal (2018) **475** 3949–3962
https://doi.org/10.1042/BCJ20180769

and refinement statistics are summarized in Table 1. The refined model was deposited in the protein data bank under the accession code 6D8V.

Isothermal titration calorimetry

$McpX^{PR}$ or $McpX^{D208N\text{-}PR}$ in 100 mM NaCl and 50 mM HEPES, pH 7.0 was used at 20 μM for the ITC (isothermal titration calorimetry) measurements with choline and proline betaine. Both ligands were dissolved in dialysis buffer. Measurements were performed with a VP-ITC Microcalorimeter (MicroCal, Northampton, MA, U.S.A.) at 15°C. $McpX^{PR}$ or $McpX^{D208N\text{-}PR}$ was placed in the sample cell. Baselines were produced by titrating the ligands into dialysis buffer void of protein. These baselines were subtracted from each protein

Table 1 Data collection and refinement statistics

The values in parentheses relate to the highest resolution shell from 2.72 to 2.7 Å. $R_{merge} = \Sigma|I| - \langle I\rangle/\Sigma I$, where I is the observed intensity and $\langle I\rangle$ is the average intensity obtained from multiple observations of symmetry-related reflections after the rejection of significant outliers. $CC_{1/2}$ = Pearson correlation coefficient between random half-datasets [50]. $R_{work} = \Sigma||F_o| - |F_c||/\Sigma|F_o|$, R_{free} defined by Brunger [51].

	$McpX^{PR}$
Wavelength (Å)	0.979
Resolution range (Å)	78.74–2.7 (2.83–2.7)
Space group	$P6_222$
Unit cell (Å)	119.04, 119.04, 121.58
Total reflections	101 395 (13 428)
Unique reflections	14 450 (1877)
Multiplicity	7.0 (7.2)
Completeness (%)	99.7 (100)
Mean *I*/sigma (*I*)	9.4 (1.7)
Wilson *B*-factor	77.10
R_{merge}	0.072 (0.766)
R_{meas}	0.080 (0.835)
CC1/2	0.998 (0.83)
Reflections used in refinement	14 121 (1348)
Reflections used for R_{free}	704 (64)
R_{work}	0.220 (0.3895)
R_{free}	0.2510 (0.3934)
CC (work)	0.945 (0.494)
CC (free)	0.951 (0.419)
Number of non-hydrogen atoms	2032
Macromolecules	2012
Ligand	18
Protein residues	269
RMS bonds (Å)	0.004
RMS angles (°)	0.60
Ramachandran favored (%)	93.63
Ramachandran allowed (%)	6.37
Average *B*-factor (Å^2)	100.6
Macromolecules	100.42
Ligands	121.53

titration. Data analysis was carried out with the MicroCal version of Origin 7.0 software using the 'one binding sites' model. (Origin Laboratory, Northampton, MA, U.S.A.).

Molecular docking

Molecular docking of the bound crystal structure ligand (proline betaine) and five additional ligands (betonicine, choline, glycine betaine, trigonelline, and proline) was performed to validate the protocol and explore binding pocking specificity of $McpX^{PR}$. The crystal structure of $McpX^{PR}$ was used as the receptor, with water molecules removed before receptor preparation in AutoDock Tools (ADT) [29]. Autodock Vina [30] was used to perform the docking and pose prediction, The same grid box co-ordinates (23 Å × 20 Å × 20 Å) and center (0.437, 0.303, 0.167) with a 1.000 Å grid spacing was used to dock all ligands and was based on the position of proline betaine in the solved structure. Nine poses for each ligand docked to $McpX^{PR}$ were generated. Our box size, center, and protocol were validated with the re-docking of proline betaine in the solved structure, producing a low-energy pose of −6.2 kcal/mol and a root-mean-square deviation (RMSD) of 1.102 Å between solved and docked proline betaine position. Notably, for all additional ligands tested, the top six energetically favorable poses had the quaternary amine group clustered at near the position as that of proline betaine. The lowest energy pose for each ligand docked was selected for further analysis to determine key interactions and residues for functionality. Distances were assessed to predict hydrogen bonding (less than 3.5 Å), electrostatic (2.5–3.5 Å), hydrophobic (3.4–3.9 Å), and distal, weaker interactions (greater than 4.0 Å) to determine the rationale for ligand specificity.

Results

The periplasmic McpX sensory region assumes a canonical dual CACHE domain fold

The overall structure of $McpX^{PR}$ assumes a dual **CA**lcium channels and **CHE**motaxis receptor (dCACHE_1) fold, wherein a membrane-proximal and a membrane-distal module are folded against the N-terminal and C-terminal halves of a long stalk helix α1, respectively (Figure 1A). The membrane-distal module (residues 65–210) contains a six-stranded, antiparallel β-sheet, which is flanked on one side by helix α2 and the C-terminal half of the stalk helix, and on the other side by helix α3. On the other side of the β-sheet, helix α3 packs against β-strands β4, β5, and β6 to create part of the proline betaine-binding pocket. The membrane-proximal module (residues 38–63, 212–306) is formed by a five-stranded antiparallel β-sheet, which is flanked on one side by helix α4 and the N-terminal half of helix α1, and by helix α5 on the other side. As has been observed in structurally related proteins, the membrane-distal and membrane-proximal modules are packed tightly against each other, suggesting an arrangement that is likely important for communicating signal binding in the distal module across the inner membrane. Although the asymmetric unit of the crystal is formed by a single $MCPX^{PR}$ molecule, application of a crystallographic symmetry axis creates a dimer (Figure 1B) that closely resembles the dimers observed for structurally homologous MCP ligand-binding domains [31–33]. The extensive dimer interface is primarily composed of a four-helix bundle formed by helix α2 and the C-terminal half of helix α1, and the equivalent regions of a symmetry-related molecule to create the dimerization interface burying a total surface area of 6836 $Å^2$ between the two molecules. A striking feature of the dimer is the approximate 25-degree kink in the stalk helix between residues 25 and 26 (Figure 1C). This kink leads to an increase in the distance between the symmetry-related stalk helices from less than 5 Å between the α-carbons of the symmetry-related Glu-65 and Glu-65′ residues just above the kink to more than 22 Å between the α-carbons of Arg-38 and Arg-38′ at the amino-terminal ends of the stalk helices. The kinking has been proposed previously to be the result of ligand binding in the membrane-distal CACHE region as a means to facilitate signal transduction upon ligand binding [31].

The ligand-binding pocket is located in the distal CACHE module

As the refinement progressed, we inspected the structure of the membrane-distal module for additional electron density in a groove that bound the small-molecule ligands in other dCACHE_1 containing receptors [31–35]. The membrane-proximal CACHE module has generally been proposed to facilitate signal transmission from the distal CACHE module to the membrane-bound regions of the receptor [1]. However, because there has been at least one instance where a small-molecule ligand bound to the membrane-proximal CACHE region [36], we also examined its putative binding pocket in $McpX^{PR}$. Both the weighted $2F_o - F_c$ and the $F_o - F_c$ electron density

Biochemical Journal (2018) **475** 3949–3962
https://doi.org/10.1042/BCJ20180769

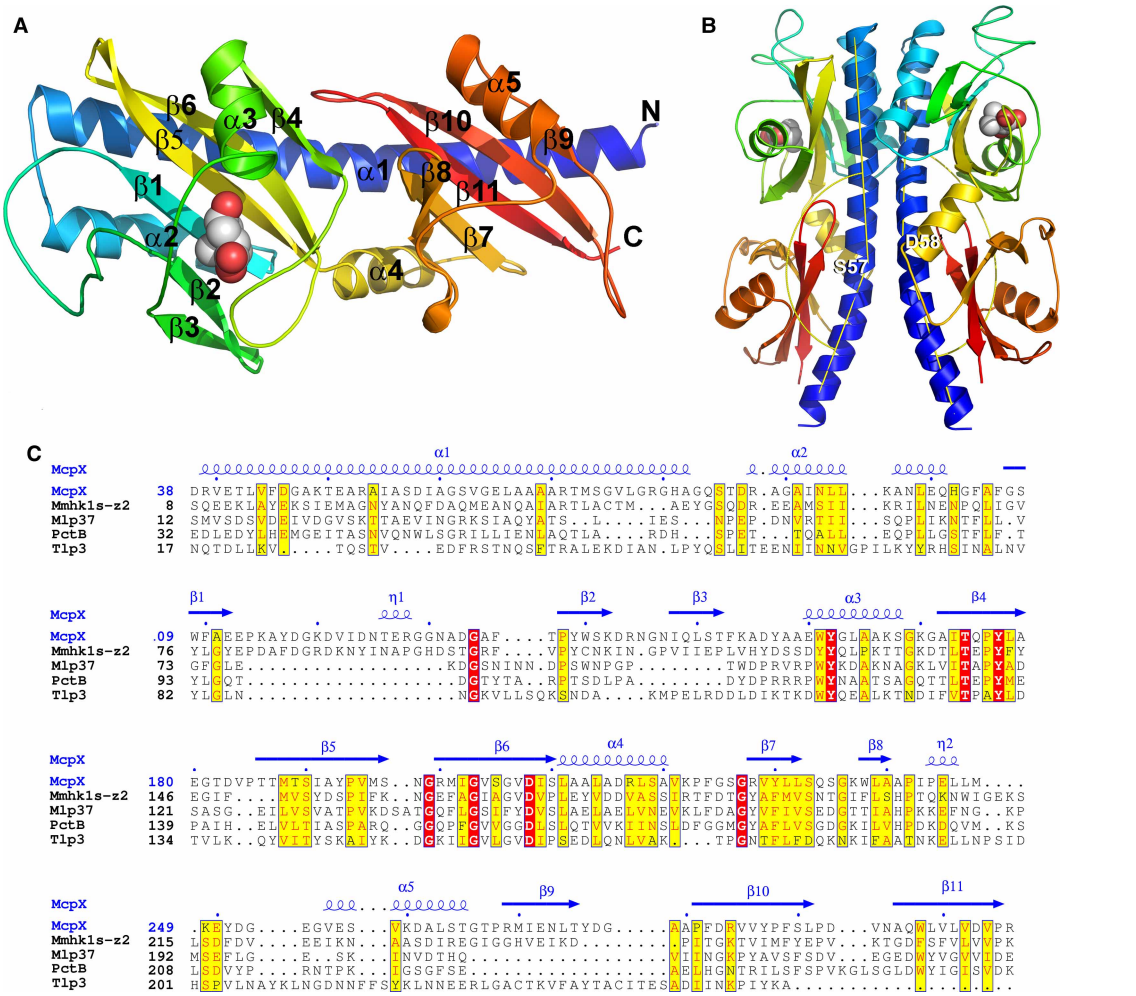

Figure 1. Structural analysis of McpX^{PR}.

(**A**) Cartoon depiction of a single McpX^{PR} molecule. Secondary structure elements are marked. Rainbow color coding tracks the backbone from the N-terminus (blue) to the C-terminus (red). Atoms of the bound proline betaine are shown as spheres. (**B**) Cartoon depiction of the McpX^{PR} dimer. The central four-helix bundle forming the dimer interface is clearly visible. Also noticeable is the pronounced kink in helix α1 that is further discussed in the text. (**C**) Structure-based sequence alignment of McpX^{PR} with other dCACHE containing sensory domains that are discussed in the text. Secondary elements of McpX^{PR} are noted above the alignment and correlate with those noted in (**A**). Strictly conserved residues are boxed red. The yellow boxes highlight residues where the chemical character of the amino acids is conserved in at least four sequences.

maps produced strong residual density in the distal CACHE region inside a groove that is formed by beta strands β1, β4, β5, the loop region connecting strand β3 and helix α3, and a 'tongue-like loop' encompassing residues 175–186 that connects strands β5 and β6 (Figures 2 and 4A). Modeling proline betaine into this density produced an excellent initial fit as judged by visual inspection. Subsequently, PHENIX was used to optimize the positioning and refine the ring conformation. In the resulting complex, the proline betaine molecule occupies the equivalent space as the serine and alanine in structures of Mlp37 from *Vibrio cholerae* [33] (PDB code: 5avf and 3c8c, respectively, Supplementary Figure S1A and B), as the isoleucine ligand in the *Campylobacter jejuni* chemoreceptor Tlp3 [32] (PDB code: 4xmr, Supplementary Figure S1C), as Bis–Tris in the putative histidine kinase mmhk1s-z2 from

Methanosarcina frisia [31] (PDB code: 3LIA, Supplementary Figure S1D), as putrescine in McpU from *Pseudomonas putida* (PDB code: 6F9G) [37] and as the arginine-ligand in the *P. aeruginosa* receptor protein PctB (PDB code: 5LT9, unpublished; Supplementary Figure S1E). One of the primary objectives of this work was to gain an understanding of the molecular basis for the unusual specificity of McpX for QACs. The

Biochemical Journal (2018) **475** 3949–3962
https://doi.org/10.1042/BCJ20180769

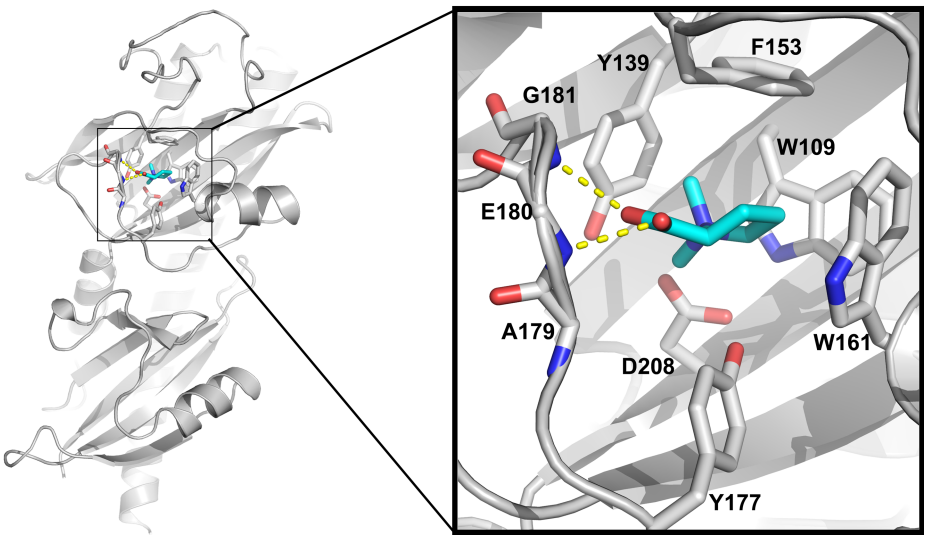

Figure 2. Close-up view of the proline betaine-binding pocket of McpX^{PR}.
Particularly noteworthy is the prevalence of interacting aromatic residues that box-in the ligand on four sides. The dashed lines mark the ~2.9 Å distance between the hydrogen-bonded amide groups from the protein and the carboxylate group of the ligand.

experimentally determined model revealed that proline betaine is co-ordinated on four sides by aromatic residues, namely Trp109, Tyr139, Phe153, and Trp161. The planes of the aromatic rings are oriented toward a positively charged amine group of the ligand creating four sets of cation–πinteractions. The carboxylate group of the ligand is stabilized by hydrogen-bonding interactions with the backbone amide groups of Ala179 and Glu180. A similar arrangement was only observed in the structure of the Bis–Tris complex of Mmhk1s-z2, where the ligand is also caged-in on four sides by aromatic residues. Three of the four tyrosines, Tyr105, Tyr135, Tyr156, in Mmhk1s-z2 structurally correspond to Trp109, Tyr139, Trp161 in McpX^{PR}. Tyr259 is located in the 'tongue-like' loop region. An additional aromatic residue, Tyr172, involved in hydrogen-bonding interactions with the ligand, and Asp199 are also conserved in McpX (Tyr177 and Asp208, respectively). In the amino acid sensor Mlp37 Trp154, Tyr170, and Asp277 (Trp161, Tyr177, Asp208 in McpX) are conserved but the serine ligand in Mlp37 is co-ordinated by charged and polar residues. In Tlp3 Tyr118, Trp150, Tyr167, Asp196 correspond to Trp109, Trp161, Tyr177, and Asp208 in McpX, but again binding of the isoleucine ligands primarily involves hydrogen-bonding and ionic interactions. The same is true for the primary amine receptor McpU in *P. putida*. In the putrescine complex of the McpU^{PR}, the ligand is co-ordinated by two aspartate residues, where Asp233 is structurally equivalent to Asp208 in McpX. Once again Tyr139 (Tyr152 in McpU), Trp161 (Trp186 in McpU), Tyr177 is also conserved in McpU (Tyr202). Lastly, in the recently solved structure of the arginine-complex of the *P. aeruginosa* receptor protein PctB (PDB code: 5LT9, unpublished), Tyr101 (Trp109 in McpX), Trp128 (Trp161 in McpX), Tyr144 (Tyr177 in McpX), and Asp173 (Asp208 in McpX) are also conserved. Because only Mmhk1s-z2 shares the box-like arrangement of aromatic residues around the ligand, it is tempting to hypothesize that the unknown ligands of the former receptor might also be QACs.

The highly conserved Asp208 residue is critical for QAC binding of McpX^{PR}

During the analysis of the ligand-binding pocket, we were struck by the conspicuous absence of interactions with charged amino acid residues in the immediate vicinity. In all other complexes, the amino acid ligands are stabilized by at least two ionic side chains from the receptor, yet in the McpX^{PR}-proline betaine complex, the carboxylate group of the ligand is hydrogen-bonded to peptide bond amides groups, while the positive charge of the amine group is co-ordinated by the π-systems of the surrounding aromatic amino acid residues. The comparison to other receptor complexes drew our attention to the highly conserved Asp208 residue. In other structures, the equivalent residue provided pivotal hydrogen-bonding contacts with the ligand, the most recent

Biochemical Journal (2018) 475 3949–3962
https://doi.org/10.1042/BCJ20180769

examples being the complex of the McpU ligand-binding domain with putrescine, where the equivalent aspartate (Asp233) interacts with a primary amine group of the ligand. However, in the $McpX^{PR}$-proline betaine complex, the positively charged amine group lacks polar hydrogen atoms and the side chain of Asp208 is positioned more than 4 Å away from that nitrogen atom (Figure 2), To determine whether or not the charge of Asp208 is nevertheless important for balancing the positive charge of the quaternary amine group, we replaced the residue with an asparagine and purified the $McpX^{D208N\text{-}PR}$ variant protein. Using ITC, we determined binding isotherms of the $McpX^{D208N\text{-}PR}$ variant for both choline and proline betaine. Remarkably, the conservative D208N mutation completely abolished binding of $McpX^{PR}$ to either ligand, demonstrating that Asp208 is essential for McpX function despite being positioned more than 4 Å away from the charged amino group of the ligand (Figure 3). The demonstrated significance of Asp208 may also explain the broad conservation of two additional residues that, at least in McpX, do not directly interact with the ligand: Ser190 forms hydrogen bonds with Tyr177 and Asp208 thus providing important second-tier contacts for shaping the binding pocket.

Molecular docking provides rationalization of the differential binding affinity of $McpX^{PR}$ for its various ligands

In a prior study, the ligand-binding properties of McpX have been profiled both qualitatively and quantitatively [21]. While the protein showed significant affinity toward only one of all proteinogenic amino acids tested, namely proline (K_D = 45.2 μM), it displayed broad specificity toward QACs, with choline being the tightest binding ligand (K_D = 138 nM) and betonicine binding with the weakest affinity (K_D = 2.3 mM) [21]. We can rationalize the 10-fold lower affinity of proline compared with the closely related proline betaine (K_D = 3.8 μM) with the fact that the ligand-binding pocket is primarily formed by aromatic residues that create a largely hydrophobic environment in that region. Therefore, the non-polar methyl groups surrounding the charged nitrogen atom provide better complementarity within the binding pocket. The difference in affinity is even greater between proline betaine and betonicine even though the only difference is an additional hydroxyl group in the C4 position of the latter. If betonicine is overlaid onto proline betaine in our experimentally determined structure, the hydroxyl group would likely force a conformational change in the ring of the ligand to avoid clashing of the hydroxyl group with the aromatic ring of Trp161 (Figure 4B). Using a molecular docking protocol validated through successful re-docking of proline betaine, one can predict a reasonably well-fitting complex with betonicine, but in that complex, the quaternary amine group of betonicine is slightly displaced. Either this displacement of the quaternary amine or a forced conformational change in the protein needed to accommodate the additional hydroxyl group could be the underlying causes for the 1000-fold reduced affinity. Additionally, we performed molecular docking studies to determine the structural basis of this selectivity not only for proline betaine (control) and betonicine but four other ligands known to bind $McpX^{PR}$, including proline, trigonelline, choline, and glycine betaine. Remarkably, despite their structural variability, the quaternary amine groups of all six ligands docked within 1 Å of the position of proline betaine in the experimental model (Figure 4C,D and Supplementary Figure S2). As the quaternary amine group constitutes the single unifying feature of all six ligands, it appears that the cation–πinteractions and ionic interactions of the quaternary amine group with Asp208 are the pivotal specificity determinants. Moreover, ligand features causing the positively charged nitrogen atom to shift from its ideal position right at the center between the four coordinating π-systems lead to a reduced binding affinity. Therefore, choline is likely the ligand with the highest affinity because its flexible backbone structure permits ideal positioning of the quaternary amine group. As discussed below, substrate-binding proteins (SBPs) involved in betaine transport also utilize cation–π interactions to bind their cognate ligands and the positions of the quaternary amine groups were observed to be highly conserved in the various QAC complexes [38–40]. The results of our modeling and docking studies show nice shape complementarity between $McpX^{PR}$ and the high-affinity ligands proline betaine, proline, choline, and glycine betaine, suggesting that they all bind in the pocket without undergoing major conformational changes or forcing changes in the protein. In the weaker binding ligands, a good fit into the ligand-binding pocket of $McpX^{PR}$ without major clashes is prevented by either a rigid ring structure (trigonelline, K_D = 88.5 μM) or by a bulky substituent (betonicine, K_D = 2.3 mM).

Discussion

dCACHE_1 domains are broadly conserved, periplasmic ligand sensing modules found in bacterial chemoreceptors and histidine kinases [23]. Generally, it is the membrane-distal CACHE domain that binds the signaling

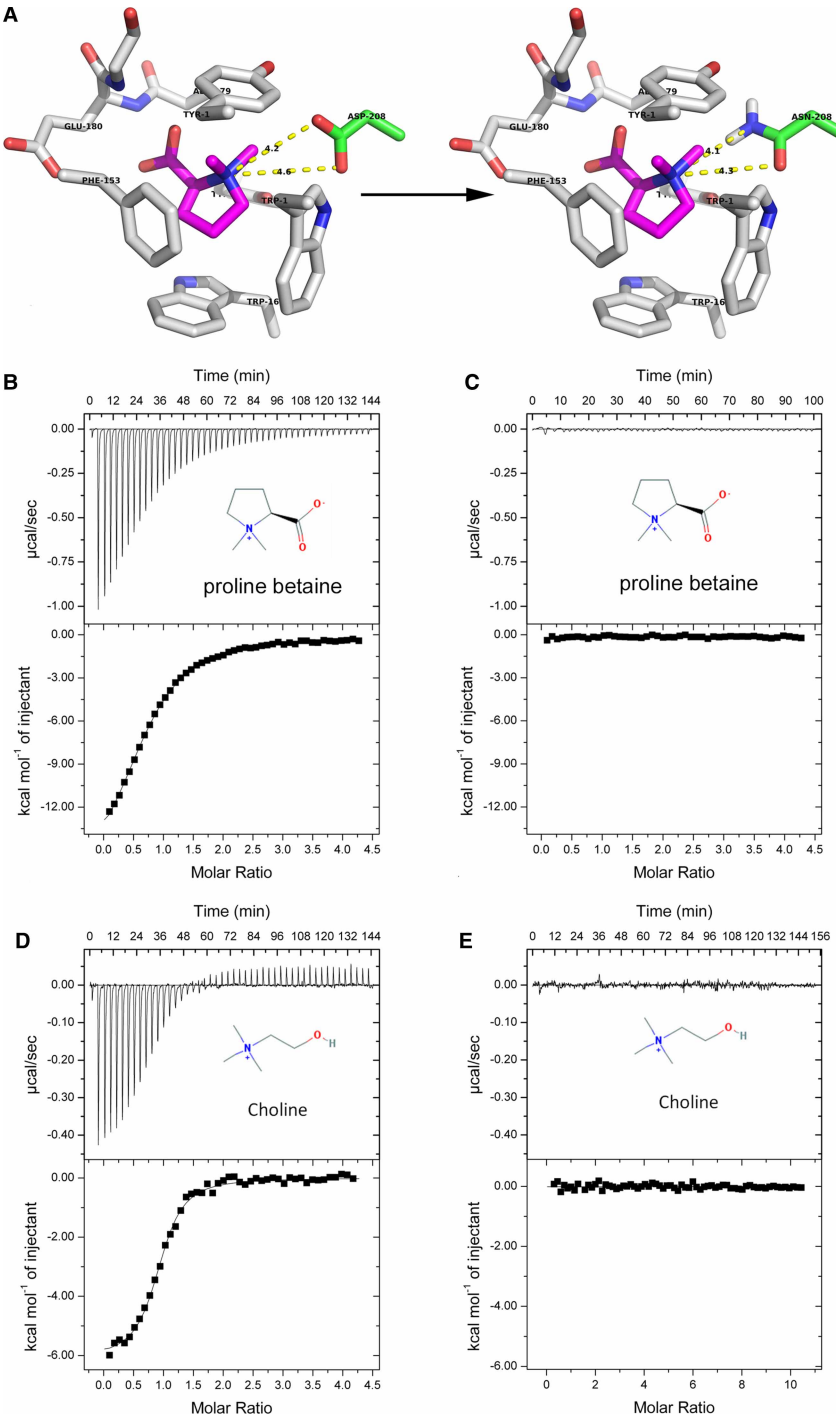

Figure 3. Role of McpX^{PR} residue D208 in ligand binding.

(**A**) Structural consequences of the D208N mutation in McpX^{PR}. (**B–E**) Results of ITC-binding studies with either the McpX^{PR} protein or the McpX$^{D208N-PR}$ variant. Upper and lower panels show the raw titration data and the isotherms derived by integrating peaks from the raw data, respectively. (**B**) Titration of McpX^{PR} with proline betaine. (**C**) Titration of McpX$^{D208N-PR}$ with proline betaine. (**D**) Titration of McpX^{PR} with choline. (**E**) Titration of McpX$^{D208N-PR}$ with choline.

ligand, while the second CACHE domain is thought to mediate signal transmission to the membrane [1]. However, it is worth noting that, in a departure from the existing paradigm, a recently discovered lactate sensor utilizes its membrane-proximal CACHE domain to directly sense lactate [36]. Ligand-binding appears to alter

Biochemical Journal (2018) **475** 3949–3962
https://doi.org/10.1042/BCJ20180769

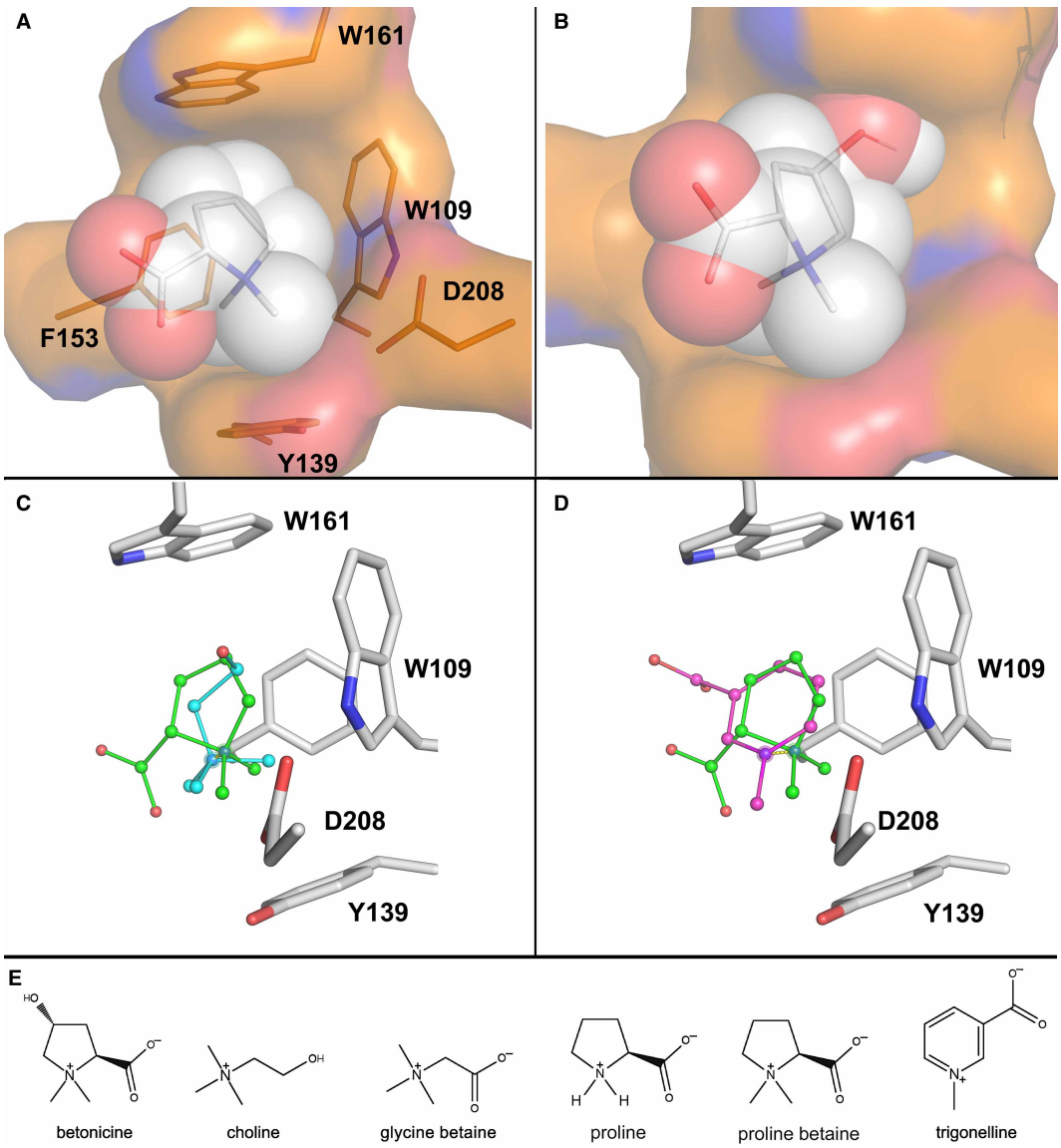

Figure 4. Possible poses of the various McpX^{PR} ligands.

(**A**) Spacefill showing the fit of the proline betaine ligand in the experimentally determined structure. Proline is expected to bind similarly, with the two methyl groups on the nitrogen being replaced with hydrogen atoms. (**B**) Space fill showing the fit of betonicine in McpX^{PR} created by adding a hydroxyl group to the experimentally fit proline betaine to demonstrate the clash of the hydroxyl group with binding site residues to explain why betonicine is bound with significantly lower affinity. (**C**) Lowest energy poses for a docked of choline McpX^{PR} complex (cyan). Proline betaine (green) is included for comparison. The two quaternary amino groups are separated by 0.6 Å. (**D**) Lowest energy pose obtained from docking trigonelline (hot pink) into the McpX^{PR} structure. Proline betaine (green) is included for comparison. The two quaternary amino groups are separated by 0.8 Å. (**E**) Schematic drawings of the discussed ligands.

the bending of the central helix causing the membrane-proximal section of the helix to be more splayed but there also appears to be a slight rotation associated with ligand binding that further separates the C-terminal ends of the two central helices in the dimer [41–45].

Although the present structure constitutes the first example of a chemotactic sensor with specificity for small QACs, we found many protein complexes in the Protein Data Bank with bound choline, glycine betaine or proline betaine. There are four entries for proline betaine complexes in the Protein Data Bank. Three of these

structures belong to SBPs that mediate the uptake of small molecules through bacterial ABC transporters. Like McpX, SBPs ProX, OpuA, OpuAC specifically target glycine betaine and proline betaine but do not facilitate amino acid transport [46]. In fact, ProX from *E. coli* is even more selective than McpX as it binds proline betaine with a K_D of ∼5 μM, while no binding of proline has been observed [40,47]. Remarkably, even though the SBP structures bear little resemblance to the structure of McpX^{PR}, the binding pockets are strikingly similar. In the structure of ligand-binding protein ProX from the hyperthermophilic archaeon *Archaeoglobus fulgidus* (PDB code 1SW1 [39]), the quaternary amine of proline betaine ligand is engaged in cation–πinteractions with four tyrosines, while the carboxylate group forms ionic interactions with Arg and Lys residues [39]. This protein was also crystallized in complex with glycine betaine (PDB code 1SW2). Glycine betaine forms the same key contacts as proline betaine and the quaternary amine groups are in the same position. In the structure of the *E. coli* ProX protein, the bound proline betaine ligand is co-ordinated by three Trp residues, while the carboxylate group is stabilized through hydrogen-bonding contacts with two backbone peptide groups and an ionic contact with a histidine side chain [48]. Again, a glycine betaine complex formed the same contacts between protein and ligand (PDB codes 1R9L and 1R9Q) [40]. The SBP OpuAC (PDB code: 2B4M) from *Bacillus subtilis* displays the same fold as ProX [38]. Here, the proline betaine ligand is also forming cation–πcontacts with three Trp residues but the carboxylate group is stabilized only through hydrogen-bonding contacts with backbone peptide groups akin to those observed in McpX. Interestingly, at least in the case of OpuAC, the closest negatively charged amino acid residue, Glu181, is 6.1 Å away from the quaternary amine group in the proline betaine complex suggesting that in this instance the ion–ion interactions are perhaps not as important as we observed in McpX (Figure 5). OpuAC was also crystallized in complex with glycine betaine (PDB code 2B4L) and the key interactions are almost identical but the absence of the ring structure from the ligand permitted the same glutamate side chain to move within 4.6 Å of the quaternary amine group.

The present work is less focused on the mechanism of signal transduction but rather on the question of how a ligand-binding module has adapted to preferentially bind small quaternary amine-containing osmolytes such as choline and proline betaine over amino acids. How does a protein maintain a strong affinity for QACs while at the same time discriminating against binding of amino acids? The answer appears to be the creation of a ligand-binding pocket rich in aromatic amino acid residues with few polar or charged amino acids in the immediate vicinity of the ligand to accommodate the unusual combination of a positive charge surrounded by hydrophobic alkyl groups as presented in QACs. Osmoprotectants such as glycine betaine and proline betaine

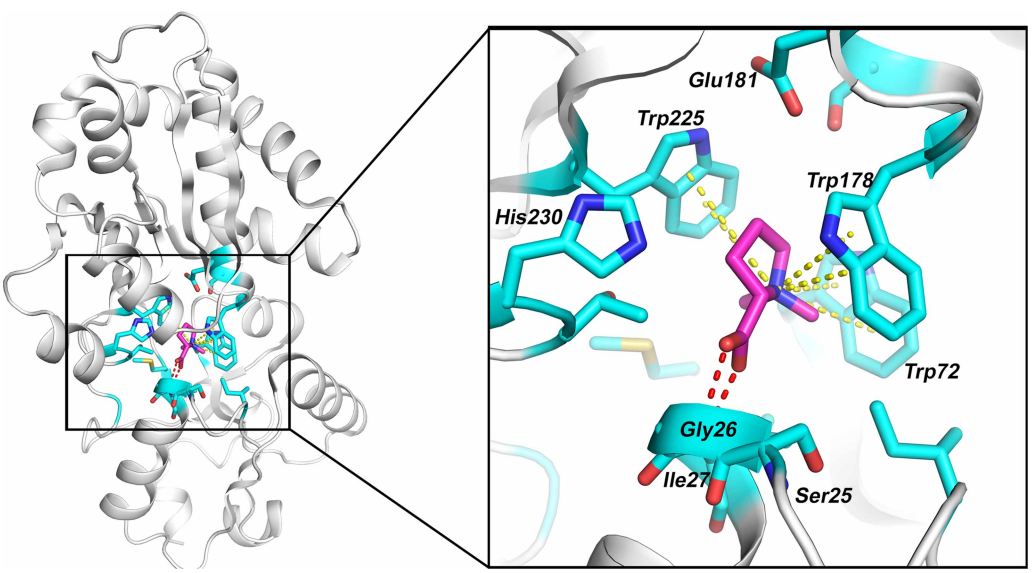

Figure 5. Overall structure and a close-up view of the proline betaine-binding pocket of the SBP OpuAC.
Noteworthy, are the similarities between the protein–ligand interactions in this structure and those observed in the McpX^{PR}-proline betaine complex.

Biochemical Journal (2018) **475** 3949–3962
https://doi.org/10.1042/BCJ20180769

are excluded from the immediate surface of proteins and are known to stabilize proteins by increasing the water concentration in the immediate vicinity of the macromolecules [49]. The sparsity of aromatic amino acids on protein surfaces stands in striking contrast with their prevalence in the binding pockets of the SBPs and McpX and thus the SBP structures provided an explanation for how a receptor can evolve affinity for a ligand that generally does not interact with proteins. Collectively, the comparison of the SBP complexes with the $McpX^{PR}$-proline betaine complex demonstrates a striking example of convergent evolution highlighting that cation–π interactions are ideal for providing binding specificity toward QACs. Both tyrosine and tryptophan residues are suitable for forming the interactions. The position of the quaternary amine group is fixed within the pocket, additional stabilizing interactions are quite variable but can serve to discriminate between QAC ligands [21,48].

Abbreviations

ADT, AutoDock Tools; dCACHE_1, dual CACHE domain; ITC, isothermal titration calorimetry; MCPs, methyl-accepting chemotaxis proteins; $McpX^{PR}$, McpX ligand-binding periplasmic region; PDB, Protein Data Bank; PMSF, phenylmethylsulfonyl fluoride; QACs, quaternary ammonium compounds; RMSD, root-mean-square deviation; SBPs, substrate-binding proteins; TCEP, tri(2-carboxyethyl)phosphine.

Author Contribution

M.S. performed the structural studies and analysis, K.K.C. isolated proteins and performed the ITC studies, J.M. M. obtained the initial crystals for McpX, assisted with the model building and manuscript, B.A.W. developed protocols for McpX purification and characterization, A.M.B. performed the molecular docking studies, B.E.S. co-wrote the manuscript, provided funding for the project and supervised the biochemical studies, F.D.S. supervised all structural and biochemical analysis, co-wrote the manuscript, and provided funding for the project.

Funding

The present study was supported by National Science Foundation grant MCB-1253234 to B.E.S and MCB-1817652 to B.E.S and F.D.S. Use of the Advanced Photon Source was supported by the U. S. Department of Energy, Office of Science, Office of Basic Energy Sciences, under Contract No. W-31-109-Eng-38.

Competing Interests

The Authors declare that there are no competing interests associated with the manuscript.

References

1 Ortega, A., Zhulin, I.B. and Krell, T. (2017) Sensory repertoire of bacterial chemoreceptors. *Microbiol. Mol. Biol. Rev.* **81**, 1–28 https://doi.org/10.1128/MMBR.00033-17
2 Matilla, M.A. and Krell, T. (2018) The effect of bacterial chemotaxis on host infection and pathogenicity. *FEMS Microbiol. Rev.* **42**, 40–67 https://doi.org/10.1093/femsre/fux052
3 Scharf, B.E., Hynes, M.F. and Alexandre, G.M. (2016) Chemotaxis signaling systems in model beneficial plant-bacteria associations. *Plant Mol. Biol.* **90**, 549–559 https://doi.org/10.1007/s11103-016-0432-4
4 Hazelbauer, G.L. (2012) Bacterial chemotaxis: the early years of molecular studies. *Annu. Rev. Microbiol.* **66**, 285–303 https://doi.org/10.1146/annurev-micro-092611-150120
5 Parkinson, J.S., Hazelbauer, G.L. and Falke, J.J. (2015) Signaling and sensory adaptation in *Escherichia coli* chemoreceptors: 2015 update. *Trends Microbiol.* **23**, 257–266 https://doi.org/10.1016/j.tim.2015.03.003
6 Hazelbauer, G.L., Falke, J.J. and Parkinson, J.S. (2008) Bacterial chemoreceptors: high-performance signaling in networked arrays. *Trends Biochem. Sci.* **33**, 9–19 https://doi.org/10.1016/j.tibs.2007.09.014
7 Berg, H.C. (2003) The rotary motor of bacterial flagella. *Annu. Rev. Biochem.* **72**, 19–54 https://doi.org/10.1146/annurev.biochem.72.121801.161737
8 Scharf, B. (2002) Real-time imaging of fluorescent flagellar filaments of *Rhizobium lupini* H13-3: flagellar rotation and pH-induced polymorphic transitions. *J. Bacteriol.* **184**, 5979–5986 https://doi.org/10.1128/JB.184.21.5979-5986.2002
9 Maddock, J.R. and Shapiro, L. (1993) Polar location of the chemoreceptor complex in the *Escherichia coli* cell. *Science* **259**, 1717–1723 https://doi.org/10.1126/science.8456299
10 Sourjik, V. and Berg, H.C. (2002) Receptor sensitivity in bacterial chemotaxis. *Proc. Natl Acad. Sci. U.S.A.* **99**, 123–127 https://doi.org/10.1073/pnas.011589998
11 Sourjik, V. and Berg, H.C. (2004) Functional interactions between receptors in bacterial chemotaxis. *Nature* **428**, 437–441 https://doi.org/10.1038/nature02406
12 Colin, R. and Sourjik, V. (2017) Emergent properties of bacterial chemotaxis pathway. *Curr. Opin. Microbiol.* **39**, 24–33 https://doi.org/10.1016/j.mib.2017.07.004

13 Gulash, M., Ames, P., Larosiliere, R.C. and Bergman, K. (1984) Rhizobia are attracted to localized sites on legume roots. *Appl. Environ. Microbiol.* **48**, 149–152
14 Soby, S. and Bergman, K. (1983) Motility and chemotaxis of *Rhizobium meliloti* in soil. *Appl. Environ. Microbiol.* **46**, 995–998
15 Caetano-Anolles, G., Wall, L.G., De Micheli, A.T., Macchi, E.M., Bauer, W.D. and Favelukes, G. (1988) Role of motility and chemotaxis in efficiency of nodulation by *Rhizobium meliloti. Plant Physiol.* **86**, 1228–1235 https://doi.org/10.1104/pp.86.4.1228
16 Meier, V.M., Muschler, P. and Scharf, B.E. (2007) Functional analysis of nine putative chemoreceptor proteins in *Sinorhizobium meliloti. J. Bacteriol.* **189**, 1816–1826 https://doi.org/10.1128/JB.00883-06
17 Meier, V.M. and Scharf, B.E. (2009) Cellular localization of predicted transmembrane and soluble chemoreceptors in *Sinorhizobium meliloti. J. Bacteriol.* **191**, 5724–5733 https://doi.org/10.1128/JB.01286-08
18 Webb, B.A., Compton, K.K., Del Campo, J.S.M., Taylor, D., Sobrado, P. and Scharf, B.E. (2017) *Sinorhizobium meliloti* chemotaxis to multiple amino acids is mediated by the chemoreceptor McpU. *Mol. Plant Microbe Interact.* **30**, 770–777 https://doi.org/10.1094/MPMI-04-17-0096-R
19 Webb, B.A., Helm, R.F. and Scharf, B.E. (2016) Contribution of individual chemoreceptors to *Sinorhizobium meliloti* chemotaxist towards amino acids of host and nonhost seed exudates. *Mol. Plant Microbe Interact.* **29**, 231–239 https://doi.org/10.1094/MPMI-12-15-0264-R
20 Webb, B.A., Hildreth, S., Helm, R.F. and Scharf, B.E. (2014) *Sinorhizobium meliloti* chemoreceptor McpU mediates chemotaxis toward host plant exudates through direct proline sensing. *Appl. Environ. Microbiol.* **80**, 3404–3415 https://doi.org/10.1128/AEM.00115-14
21 Webb, B.A., Compton, K.K., Castañeda Saldaña, R., Arapov, T., Ray, W.K., Helm, R.F. et al. (2017) *Sinorhizobium meliloti* chemotaxis to quaternary ammonium compounds is mediated by the chemoreceptor McpX. *Mol. Microbiol.* **103**, 333–346 https://doi.org/10.1111/mmi.13561
22 Welsh, D.T. (2000) Ecological significance of compatible solute accumulation by micro-organisms: from single cells to global climate. *FEMS Microbiol. Rev.* **24**, 263–290 https://doi.org/10.1111/j.1574-6976.2000.tb00542.x
23 Upadhyay, A.A., Fleetwood, A.D., Adebali, O., Finn, R.D. and Zhulin, I.B. (2016) Cache domains that are homologous to, but different from PAS domains comprise the largest superfamily of extracellular sensors in prokaryotes. *PLoS Comput. Biol.* **12**, e1004862 https://doi.org/10.1371/journal.pcbi.1004862
24 Zhulin, I.B., Nikolskaya, A.N. and Galperin, M.Y. (2003) Common extracellular sensory domains in transmembrane receptors for diverse signal transduction pathways in bacteria and archaea. *J. Bacteriol.* **185**, 285–294 https://doi.org/10.1128/JB.185.1.285-294.2003
25 Anantharaman, V. and Aravind, L. (2000) Cache - a signaling domain common to animal $Ca(2^+)$-channel subunits and a class of prokaryotic chemotaxis receptors. *Trends Biochem. Sci.* **25**, 535–537 https://doi.org/10.1016/S0968-0004(00)01672-8
26 Anantharaman, V., Koonin, E.V. and Aravind, L. (2001) Regulatory potential, phyletic distribution and evolution of ancient, intracellular small-molecule-binding domains. *J. Mol. Biol.* **307**, 1271–1292 https://doi.org/10.1006/jmbi.2001.4508
27 Adams, P.D., Afonine, P.V., Bunkóczi, G., Chen, V.B., Davis, I.W., Echols, N. et al. (2010) *PHENIX*: a comprehensive Python-based system for macromolecular structure solution. *Acta Crystallogr. D Biol. Crystallogr.* **66**(Pt 2), 213–221 https://doi.org/10.1107/S0907444909052925
28 Karplus, P.A. and Diederichs, K. (2015) Assessing and maximizing data quality in macromolecular crystallography. *Curr. Opin. Struct. Biol.* **34**, 60–68 https://doi.org/10.1016/j.sbi.2015.07.003
29 Morris, G.M., Huey, R., Lindstrom, W., Sanner, M.F., Belew, R.K., Goodsell, D.S. et al. (2009) Autodock4 and AutoDockTools4: automated docking with selective receptor flexibility. *J. Comput. Chem.* **30**, 2785–2791 https://doi.org/10.1002/jcc.21256
30 Trott, O. and Olson, A.J. (2010) Autodock Vina: improving the speed and accuracy of docking with a new scoring function, efficient optimization, and multithreading. *J. Comput. Chem.* **31**, 455–461 PMID:19499576
31 Zhang, Z. and Hendrickson, W.A. (2010) Structural characterization of the predominant family of histidine kinase sensor domains. *J. Mol. Biol.* **400**, 335–353 https://doi.org/10.1016/j.jmb.2010.04.049
32 Liu, Y.C., Machuca, M.A., Beckham, S.A., Gunzburg, M.J. and Roujeinikova, A. (2015) Structural basis for amino-acid recognition and transmembrane signalling by tandem Per-Arnt-Sim (tandem PAS) chemoreceptor sensory domains. *Acta Crystallogr. D Biol. Crystallogr.* **71**(Pt 10), 2127–2136 https://doi.org/10.1107/S139900471501384X
33 Nishiyama, S.-., Takahashi, Y., Yamamoto, K., Suzuki, D., Itoh, Y., Sumita, K. et al. (2016) Identification of a *Vibrio cholerae* chemoreceptor that senses taurine and amino acids as attractants. *Sci. Rep.* **6**, 20866 https://doi.org/10.1038/srep20866
34 Glekas, G.D., Mulhern, B.J., Kroc, A., Duelfer, K.A., Lei, V., Rao, C.V. et al. (2012) The *Bacillus subtilis* chemoreceptor McpC senses multiple ligands using two discrete mechanisms. *J. Biol. Chem.* **287**, 39412–39418 https://doi.org/10.1074/jbc.M112.413518
35 Rico-Jiménez, M., Muñoz-Martínez, F., Garcia-Fontana, C., Fernandez, M., Morel, B., Ortega, A. et al. (2013) Paralogous chemoreceptors mediate chemotaxis towards protein amino acids and the non-protein amino acid gamma-aminobutyrate (GABA). *Mol. Microbiol.* **88**, 1230–1243 https://doi.org/10.1111/mmi.12255
36 Machuca, M.A., Johnson, K.S., Liu, Y.C., Steer, D.L., Ottemann, K.M. and Roujeinikova, A. (2017) *Helicobacter pylori* chemoreceptor TlpC mediates chemotaxis to lactate. *Sci. Rep.* **7**, 14089 https://doi.org/10.1038/s41598-017-14372-2
37 Gavira, J.A., Ortega, A., Martín-Mora, D., Conejero-Muriel, M.T., Corral-Lugo, A., Morel, B. et al. (2018) Structural basis for polyamine binding at the dCACHE domain of the McpU chemoreceptor from *Pseudomonas putida. J. Mol. Biol.* **430**, 1950–1963 https://doi.org/10.1016/j.jmb.2018.05.008
38 Horn, C., Sohn-Bösser, L., Breed, J., Welte, W., Schmitt, L. and Bremer, E. (2006) Molecular determinants for substrate specificity of the ligand-binding protein OpuAC from *Bacillus subtilis* for the compatible solutes glycine betaine and proline betaine. *J. Mol. Biol.* **357**, 592–606 https://doi.org/10.1016/j.jmb.2005.12.085
39 Schiefner, A., Holtmann, G., Diederichs, K., Welte, W. and Bremer, E. (2004) Structural basis for the binding of compatible solutes by ProX from the hyperthermophilic archaeon *Archaeoglobus fulgidus. J. Biol. Chem.* **279**, 48270–48281 https://doi.org/10.1074/jbc.M403540200
40 Schiefner, A., Breed, J., Bösser, L., Kneip, S., Gade, J., Holtmann, G. et al. (2004) Cation-pi interactions as determinants for binding of the compatible solutes glycine betaine and proline betaine by the periplasmic ligand-binding protein ProX from *Escherichia coli. J. Biol. Chem.* **279**, 5588–5596 https://doi.org/10.1074/jbc.M309771200
41 Ames, P., Hunter, S. and Parkinson, J.S. (2016) Evidence for a helix-clutch mechanism of transmembrane dignaling in a bacterial chemoreceptor. *J. Mol. Biol.* **428**, 3776–3788 https://doi.org/10.1016/j.jmb.2016.03.017
42 Ottemann, K.M., Xiao, W., Shin, Y.K. and Koshland, Jr., D.E. (1999) A piston model for transmembrane signaling of the aspartate receptor. *Science* **285**, 1751–1754 https://doi.org/10.1126/science.285.5434.1751

Biochemical Journal (2018) **475** 3949–3962
https://doi.org/10.1042/BCJ20180769

43 Yu, D., Ma, X., Tu, Y. and Lai, L. (2015) Both piston-like and rotational motions are present in bacterial chemoreceptor signaling. *Sci. Rep.* **5**, 8640 https://doi.org/10.1038/srep08640
44 Chervitz, S.A. and Falke, J.J. (1996) Molecular mechanism of transmembrane signaling by the aspartate receptor: a model. *Proc. Natl Acad. Sci. U.S.A.* **93**, 2545–2550 https://doi.org/10.1073/pnas.93.6.2545
45 Gushchin, I., Melnikov, I., Polovinkin, V., Ishchenko, A., Yuzhakova, A., Buslaev, P. et al. (2017) Mechanism of transmembrane signaling by sensor histidine kinases. *Science* **356**, eaah6345 https://doi.org/10.1126/science.aah6345
46 Haardt, M., Kempf, B., Faatz, E. and Bremer, E. (1995) The osmoprotectant proline betaine is a major substrate for the binding-protein-dependent transport system ProU of *Escherichia coli* K-12. *Mol. Gen. Genet.* **246**, 783–786 https://doi.org/10.1007/BF00290728
47 Barron, A., Jung, J.U. and Villarejo, M. (1987) Purification and characterization of a glycine betaine binding protein from *Escherichia coli*. *J. Biol. Chem.* **262**, 11841–6
48 Smits, S.H., Hoing, M., Lecher, J., Jebbar, M., Schmitt, L. and Bremer, E. (2008) The compatible-solute-binding protein OpuAC from *Bacillus subtilis*: ligand binding, site-directed mutagenesis, and crystallographic studies. *J. Bacteriol.* **190**, 5663–5671 https://doi.org/10.1128/JB.00346-08
49 Horn, C., Jenewein, S., Sohn-Bösser, L., Bremer, E. and Schmitt, L. (2005) Biochemical and structural analysis of the *Bacillus subtilis* ABC transporter OpuA and its isolated subunits. *J. Mol. Microbiol. Biotechnol.* **10**, 76–91 https://doi.org/10.1159/000091556
50 Karplus, P.A. and Diederichs, K. (2012) Linking crystallographic model and data quality. *Science* **336**, 1030–1033 https://doi.org/10.1126/science.1218231
51 Brünger, A.T. (1992) Free R value: a novel statistical quantity for assessing the accuracy of crystal structures. *Nature* **355**, 472–475 https://doi.org/10.1038/355472a0